JOC The Journal of Organic Chemistry

Article

pubs.acs.org/joc

Dynamic Behavior, Electrochromism, and Two-Photon Absorption of Dicyanomethylenated Quinacridone

Takashi Takeda,*[,†] Hiroyuki Sugihara,[‡] Yasutaka Suzuki,[‡] Jun Kawamata,[‡] and Tomoyuki Akutagawa*[,†]

[†]Institute of Multidisciplinary Research for Advanced Materials, Tohoku University, Katahira 2-1-1, Sendai, Miyagi 980-8577, Japan

[‡]Graduate School of Medicine, Yamaguchi University, Yoshida 1677-1, Yamaguchi, Yamaguchi 753-8512, Japan

Supporting Information

ABSTRACT: Molecular structures of dicyanomethylenated quinacridone (**1**) as a solid and in solution were examined on the basis of single-crystal X-ray structural analysis, temperature-dependent ^{1}H NMR in CD_2Cl_2, and theoretical calculations. Crystal **1** had a curved, butterfly-shaped molecular structure. Thermally activated flipping between the curved, butterfly-shaped structure and an armchair structure occurred in solution. Electrochemical reduction triggered a dynamic change from the curved, butterfly-shaped conformation in the neutral state to a planar conformation in the dianion state, which represented electrochromic behavior with electrochemical bistability. A large two-photon absorption cross section of compound **1** was observed in the resonance-enhancement region of 423 GM (1 GM = 1×10^{-50} cm^4 s photon^{-1} molecule^{-1}) at 710 nm. Multiple donor−acceptor charge-transfer pathways of molecule **1** enhanced two-photon absorption.

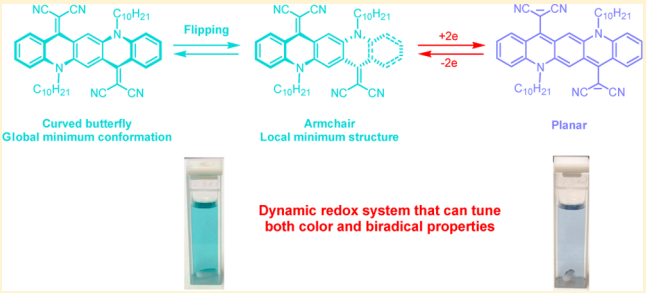

INTRODUCTION

It is important that we understand and learn to control molecular motion so that unique physical properties of materials can be expressed. For instance, molecular motion in molecular assemblies affects intermolecular interactions and thus bulk solid-state properties such as electrical conduction as well as magnetic and dielectric properties. Although full control of molecular motion in molecular assemblies has not yet been achieved, a few important solid-state molecular rotator−stator structures have been constructed.[1−3] In some cases, bulk physical properties have been successfully manipulated by controlling molecular motion. For instance, molecular rotation was coupled with ferroelectricity in a supramolecular crystal of (*m*-fluoroanilium)(dibenzo[18]crown-6)[Ni(dmit)$_2$], whereby dipole inversion was realized by the 2-fold flip-flop motion of *m*-fluoroanilinium under the application of an electric field.[4]

As in the solid state, it is also important to control the dynamic behavior of molecules in solution, which could affect electronic, aggregational, and photophysical properties. In contrast to the solid state, various types of motional freedom are allowed in solution because of the lack of restrictions that result from intermolecular steric repulsion in a close-packed crystal structure. Elaborate dynamic behavior in solution has been reported, such as a shuttling motion of rotaxanes,[5] gear motion of triptycenes,[6] and so forth. The dynamic behavior of strained, π-conjugated hydrocarbons has recently been studied extensively using bowl-shaped, π-conjugated carbon molecules such as sumanene and corranulene,[7] which undergo a bowl-to-bowl flipping motion depending on the depth of the bowl.[7d] However, there have been few studies addressing the flipping motions of simple twisted acene derivatives in solution.

An interesting method for coupling molecular motions with physical responses in solution is a dynamic redox system.[8] Conformational changes of the π-electronic core due to redox processes affect the electronic nature of the molecule, which results in electrochromic behavior with electrochemical bistability.[9,10] For instance, the butterfly-shaped molecular conformation of 11,11,12,12-tetracyanoanthra-9,10-quinodimethane (TCNAQ) in a neutral state was transformed to a planar structure in a dianionic state through two-electron reduction. The C═C double-bond character of dicyanomethylene C═C(CN)$_2$ groups in neutral TCNAQ was transformed to C−C single bonds by reduction, which relaxed the steric hindrance between C═C(CN)$_2$ groups and hydrogen atoms of neighboring benzene rings in the dianion state. This dynamic structural change could be monitored by UV−vis and fluorescence spectra.[11] The development of an electroactive, dynamic π-electron system other than TCNAQ has the potential to form a new dynamic redox system.

Quinacridone (QAcrd), an aromatic pentacyclic diaminodiketone, has been used as a low-cost, durable pigment in paints and inks (Scheme 1). QAcrd derivatives have been shown to have excellent photophysical and electronic properties, which have been applied to emitting materials in organic light-emitting diodes[12,13] and photoconductive devices.[14] Therefore, the electronic and optical properties of QAcrd derivatives are

Received: August 4, 2014
Published: September 25, 2014

Scheme 1. Dicyanomethylene-Substituted QAcrd Derivative (1), Dicyanomethylene-Substituted Acrd Derivative (2), and Their Precursors (3 and 4)

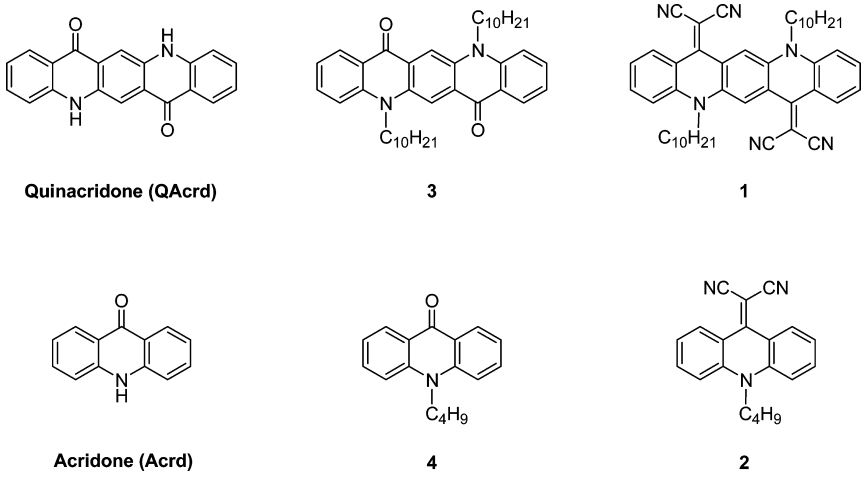

promising candidates for coupling with dynamic molecular motion. Because QAcrd itself has a planar structure, modification of this structure is necessary to construct a dynamic system. The introduction of units that impart steric hindrance into the parent molecular framework to form a twisted structure should be a straightforward method for obtaining a dynamic electronic system. A dicyanomethylene-substituted QAcrd derivative will form a twisted molecular structure because of steric hindrance between the $C{=}C(CN)_2$ groups and neighboring hydrogen atoms, whereas the electrochemically reduced dianionic states should be planar as a result of the rotation of the $C{-}C(CN)_2$ groups (Scheme 2). Another

Scheme 2. Change in Conformation between Neutral 1 and Two-Electron-Reduced 1^{2-}

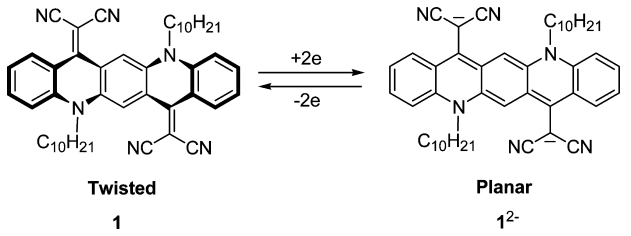

point of interest regarding twisted QAcrd derivatives is their dynamic behavior in solution. Twisted acene molecules with a low symmetry of C_i and/or C_2 point groups should enable us to use the simple spectroscopic method of variable-temperature NMR to evaluate the flipping motion in solution.

In this study, we focused on the ability of a dicyanomethylene-substituted QAcrd derivative (**1**) to function as a new dynamic redox system. In addition to its dynamic equilibrium in solution and electrochemical properties, **1** would be an interesting motif for two-photon absorption (TPA) studies because two antiparallel intramolecular charge-transfer (CT)-type transition dipole moments exist along the short axis of the molecule. With regard to potential applications in fine 3D modeling, medical markers, and future data storage devices,[15] molecules with a large TPA cross section have attracted significant attention. Various types of π molecules have been shown to exhibit relatively large TPA properties and have been used to excite molecules with three-dimensional space selectivity and high resolution.[16−18] Among these chemical designs, the highly polarized D−A π-system is useful for increasing the magnitude of intramolecular CT interactions and the TPA cross section. Multiple intramolecular CT systems in particular, such as A-π-D-π-A and D-π-A-π-D molecules, have been used to construct useful TPA materials.[18] This suggests that a molecule with multiple π-conjugated pathways such as **1** may exhibit significant TPA properties. It would be interesting to determine if dynamic equilibrium could be controlled selectively in three dimensions by an external stimulus. In this regard, TPA should be an ideal external stimulus because it can cause regioselective thermal excitation. Thus, the investigation of compounds with both dynamic equilibrium and TPA properties is intriguing. Because QAcrd itself is insoluble in common organic solvents, two decyl chains ($-C_{10}H_{21}$) were introduced into the two amino nitrogen sites of the QAcrd framework to improve its solubility. The dicyanomethylene-substituted acridone (**2**), which is essentially half of the structural unit of QAcrd, was also investigated to compare its structural and optoelectronic properties with those of **1**. The molecular structures in the solid state, dynamic behaviors in solution, redox properties, and TPA properties of molecules **1** and **2** were examined .

RESULTS AND DISCUSSION

Compound **1** and dianion $\mathbf{1}^{2-}$ were expected to show twisted and planar conformations, respectively, (Scheme 2) because of the conformational restriction imposed by the $C{=}C(CN)_2$ groups. Although Wang and co-workers[19] reported the electronic spectrum of dicyanomethylated QAcrd with C_4H_9/C_6H_{13}/C_8H_{17} groups on the nitrogens in a thin film, its HOMO−LUMO energy level and application to solution-processable organic bulk heterojunction solar cells, crystal structure, self-assembly, dynamic properties, and optoelectronic properties have not yet been examined. The dynamic flipping motion of the highly strained, curved, butterfly-shaped molecule **1** was examined in solution using variable-temperature ^{1}H NMR, which revealed structural equilibrium between the curved, butterfly-shaped conformation with a global energy minimum and an armchair-shaped conformation with a local energy minimum. The two-electron reduction of **1** yielded dianion $\mathbf{1}^{2-}$ with moderate biradical character, where the rotation of C−C single bonds around the $C{-}C(CN)_2$ groups changed the molecular conformation from a butterfly to a

dx.doi.org/10.1021/jo501800g | J. Org. Chem. 2014, 79, 9669−9677

planar conformation. A large TPA cross section for molecule **1** was observed in the resonance-enhancement region of 423 GM (1 GM = 1 × 10^{-50} cm^4 s $photon^{-1}$ $molecule^{-1}$) at 710 nm. Multiple donor−acceptor CT pathways in molecule **1** enhanced its TPA properties.

Preparation of 1 and 2 and Their Molecular Structures in the Crystalline State. Dicyanomethylenated QAcrd (**1**) and Acrd (**2**) were prepared by the alkylation of commercially available QAcrd and Acrd, followed by condensation with malononitrile in acetic anhydride at high temperature. Condensation of **3** with malononitrile at a temperature below 140 °C resulted in a mixture of **1** and its monodicyanomethylenated derivative, which were difficult to separate.

To confirm the effects of expansion in the π-electron system and the bifused molecular structure, we investigated the crystal structures of **1** and **2**. The molecular structures of **1** and **2** were evaluated by single-crystal X-ray structural analyses at 100 K. The $C_{46}H_{52}N_6$ and $C_{20}H_{17}N_3$ units in crystals of **1** and **2**, respectively, were crystallographically independent structural units within the unit cell. Figure 1 summarizes the molecular

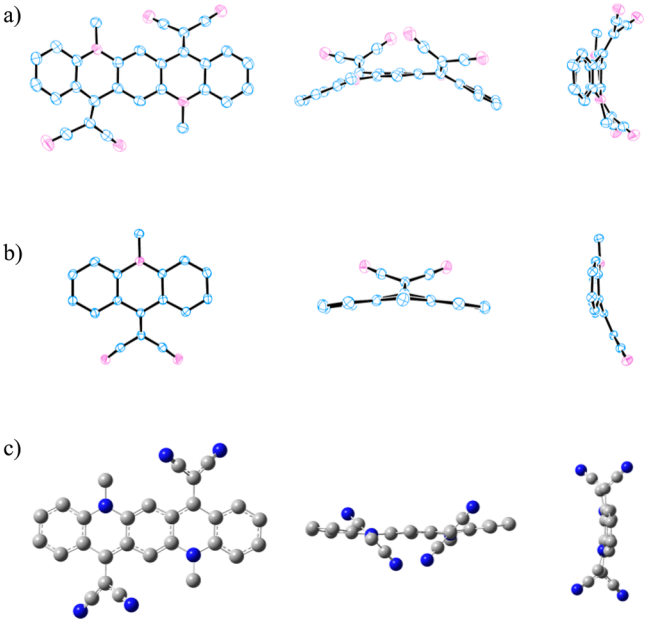

Figure 1. Molecular structures of **1**, **2**, and dianion $\mathbf{1}^{2-}$. ORTEP drawings of the structures of (a) **1** and (b) **2** based on single-crystal X-ray structural analyses. Alkyl chains and hydrogen atoms were omitted for clarity. (c) Optimized structure of dianion $\mathbf{1}^{2-}$ using a DFT calculation with the B3LYP/6-31G* basis set. $C_{10}H_{21}$ groups were replaced by CH_3 groups in the calculations. Drawings on the left, center, and right show the molecular structures of the molecules as viewed from the direction normal to the π plane, short axis, and long axis, respectively.

structures of **1** and **2** viewed normal to the π plane (left), short axis (center), and long axis of the molecules (right). Table 1 summarizes selected dihedral and torsion angles of molecules **1** and **2**. Molecule **1** showed a highly distorted butterfly-shaped conformation in the crystalline state, where the terminal benzene rings were bent in a direction opposite to the dicyanomethylene groups (Figure 1a). This highly twisted molecular structure was demonstrated by the large dihedral angles between the two benzene rings [θ_{AB} = 21.6(1)° and θ_{BC} = 29.4(1)°] and the torsion angles around the C═C(CN)$_2$

Table 1. Dihedral and Torsion Angles of 1, Dianion $\mathbf{1}^{2-}$, 2, and TCNAQ as a Reference

compound	**1**	$\mathbf{1}^{2-}$ (opt.)[a]	**2**	TCNAQ[b]
θ_{AB}[c]	21.6(1)	7.00	15.7(1)	35.4
θ_{BC}[c]	29.4(1)			
ϕ[c]	32.0(3)	4.34	25.2(3)	25.8
ϕ'[c]	34.2(3)			
ϕ''[c]	4.1(4)	45.6	1.4(4)	4.83
ϕ'''[c]	1.9(5)			

[a]The molecular structure of dianion $\mathbf{1}^{2-}$ was optimized using a DFT calculation with the B3LYP/6-31G* basis set. [b]11,11,12,12-Tetracyanoanthra-9,10-quinodimethane. See ref 21. [c]Three planes in **1** (A, B, and C) and two planes in **2** (A and B) were defined as below. The dihedral angles of A ≈ B and B ≈ C planes were θ_{AB} and θ_{BC}, respectively. The dihedral angles of the dicyanomethylene units (ϕ, ϕ', ϕ'', and ϕ''') were defined as C_A−C_B−C_C−C_D, C_A'−C_B'−C_C'−C_D', C_B−C_C−C_D−C_E, and C_B'−C_C'−C_D'−C_E' bonds in **1** and **2**, respectively.

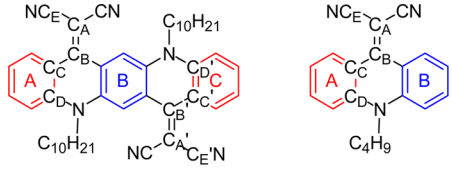

groups [ϕ = 32.0(3)° and ϕ' = 34.2(3)°] (Table 1). Because QAcrd and dialkoxy-QAcrd derivatives have been reported to have planar molecular structures in crystals,[20] the two C═C(CN)$_2$ groups were considered to play an important role in the curved, butterfly-shaped π-bending conformation of **1**. The dihedral (θ_{AB} and θ_{BC}) and torsion (ϕ and ϕ') angles of molecule **1** were similar to those of TCNAQ (θ_{AB} = 35.4° and ϕ = 25.8°).[21] In contrast, whereas the dicyanomethylene-substituted Acrd derivative **2** also showed a butterfly-shaped conformation, the magnitude of the distortion [θ_{AB} = 15.7(1)° and ϕ' = 25.2(3)°] was less than that seen in molecule **1** (Figure 1b). This is additional evidence that dicyanomethylene groups generate steric repulsion to form a highly twisted structure in **1**.

To estimate the molecular structure of dianionic species $\mathbf{1}^{2-}$, its molecular structure was optimized by a DFT calculation with the B3LYP/6-31G* basis set (Figure 1c). The two-electron reduction of molecule **1** changed the C═C(CN)$_2$ double-bond character to C−C(CN)$_2$ single bonds, resulting in rotational freedom of the C−C(CN)$_2$ groups, which reduces the steric repulsion around them. In fact, the structural parameters [θ_{AB} = 7.00° and ϕ = 4.34°] in the optimized structure of $\mathbf{1}^{2-}$ were significantly smaller than those in **1**. The dihedral angle between terminal benzene rings A and C, another parameter of molecular twisting, was also greatly reduced from 50° in the neutral state (**1**) to 15° in the dianion state ($\mathbf{1}^{2-}$). This result demonstrates that two-electron reduction produced a dynamic change in the structure of **1**.

Dynamic Behavior in Solution. Because the self-aggregating behaviors of *N*,*N*′-dialkyl-QAcrd derivatives in nonpolar solvents have already been reported spanning millimolar concentration ranges,[22] we first examined its concentration-dependent ^{1}H NMR spectra in $CDCl_3$ at room temperature. However, no changes were seen in the chemical shifts of ^{1}H NMR spectra of **1** in $CDCl_3$ in the concentration range from 0.85 to 31.2 mM (Figure S5 in the Supporting Information (SI)). These results show that a structural change

dx.doi.org/10.1021/jo501800g | J. Org. Chem. 2014, 79, 9669−9677

in the QAcrd core to a twisted conformation effectively suppresses self-aggregation in solution.

Temperature-dependent ^{1}H NMR was performed for **1** in CD_2Cl_2 at a concentration of 5.7 mM to investigate its flipping motion in solution. Peaks corresponding to the five aromatic protons (H_a, H_b, H_c, H_d, and H_e in Figure 2) were observed

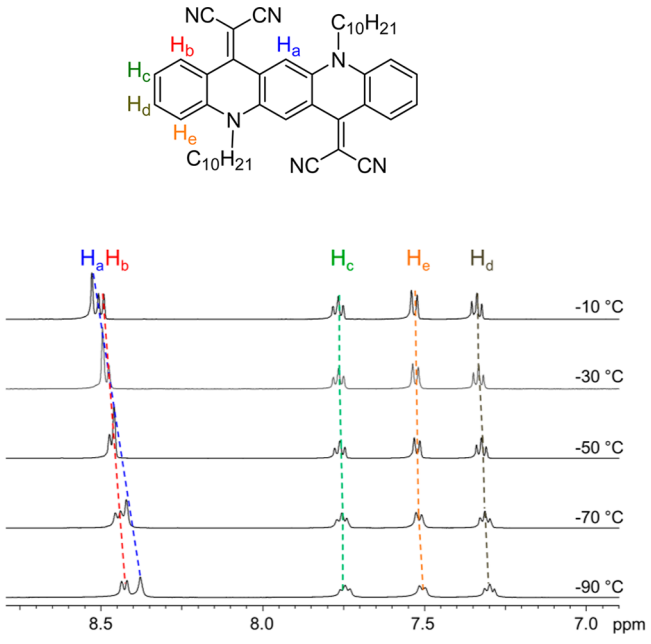

Figure 2. Temperature-dependent ^{1}H NMR spectra of **1** in CD_2Cl_2 (5.7 mM) at temperatures ranging from −90 to −10 °C.

within a range of chemical shifts (δ) from 7 to 9 ppm. When the temperature was reduced from −10 to −90 °C, the spectral shapes became broader, which suggested rapid molecular motion at high temperatures and deceleration at low temperatures. Additionally, the magnitude of the high-field shift of the H_a proton on the central benzene ring with a decrease in temperature was greater than that of the other aromatic protons, which suggests the existence of a dynamic structural equilibrium in solution. Although the ^{1}H NMR spectra of QAcrd **1** at lower temperatures is of interest in observing coalescence, we could not conduct variable-temperature NMR spectra below −90 °C because of equipment constraints and solvent limitations.

The dynamic behavior of **1** was evaluated using DFT calculations with the B3LYP/6-31G* basis set. We assumed that two kinds of flipping motion occurred in molecule **1**. The first was flipping from an up- to a down-butterfly conformation, and the second was from a butterfly to an armchair conformation (Scheme 3). The latter requires the flipping of one of the two terminal benzene rings and one C═C(CN)$_2$ group, whereas the former motion requires the flipping of both benzene rings and two C═C(CN)$_2$ groups simultaneously. The activation energies of these flipping motions were theoretically evaluated in terms of the torsion angles at C_A−C_B−C_C−C_D (ϕ) and C_A'−C_B'−C_C'−C_D' (ϕ') in molecules **1** and **2**, respectively.

Figure 3b shows the potential energy curve for the symmetrical twisting of two C═C(CN)$_2$ groups starting from a planar structure, where structural parameters ϕ and ϕ' are equal to each other. The model calculation corresponded to the transformation from an up- to a down-butterfly conformation. The relative energy (ΔE) was obtained for every 5° interval from $\phi = \phi' = 0°$ (planar structure) to $\phi = \phi' = 45°$ (twisted structure), where the ΔE value at $\phi = \phi' = 0°$ was defined as $\Delta E = 0$. The ΔE−ϕ plot shows a single-minimum potential energy curve with a minimum potential energy at $\phi = \phi' \approx 30°$, which is consistent with the molecular structure from X-ray crystal structural analysis with $\phi = 32.0°$ and $\phi' = 34.2°$. The potential energy barrier of ∼10 kcal mol^{-1} between the planar and twisted conformations is quite small and is similar to the flipping barrier (∼11 kcal mol^{-1}) for cyclohexane.[23]

These motions were easily activated by thermal energy at around room temperature ($k_BT \approx 0.6$ kcal mol^{-1} at 300 K). Therefore, the flipping motion could be easily activated at around room temperature. A similar single-minimum potential energy curve was observed in molecule **2** (red squares in Figure 3b), where the potential energy barrier (∼5 kcal mol^{-1}) for flipping the C═C(CN)$_2$ group was about half that required for molecule **1**. The dihedral angle of **2** in the X-ray crystal structural analysis was $\phi = 25.2°$, which is consistent with the theoretical value (energy minimum at $\phi = 30°$).

We fixed the conformation of one C═C(CN)$_2$ group in molecule **1** at the optimized value of $\phi = 31°$ and then evaluated the ΔE by ϕ' plots to confirm the potential existence of an armchair conformation with another local minimum potential energy (Figure 3c). A local energy minimum was observed at a dihedral angle (ϕ') of approximately −30°, which corresponds to an armchair conformation with an upper and lower C═C(CN)$_2$ arrangement relative to the π-plane of QAcrd. The energy difference between the global energy minimum curved, butterfly-shaped conformation and the

Scheme 3. Two Stable Conformations, a Curved, Butterfly-Shaped Conformation (Global Energy Minimum) and an Armchair Conformation (Local Energy Minimum), for 1 in Solution

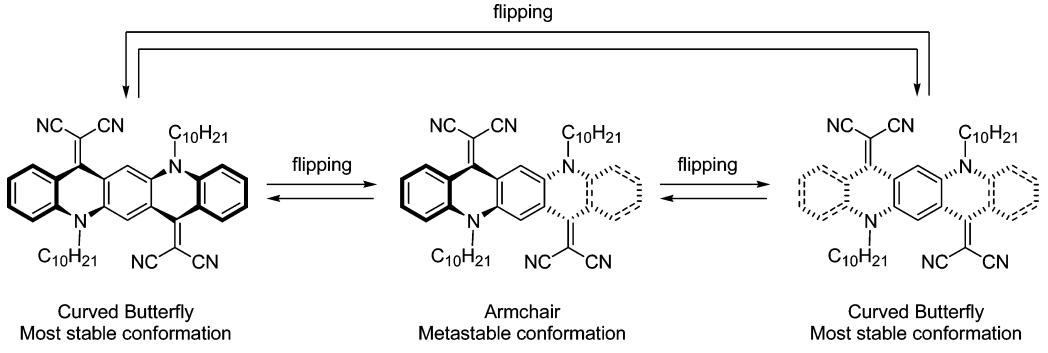

dx.doi.org/10.1021/jo501800g | J. Org. Chem. 2014, 79, 9669−9677

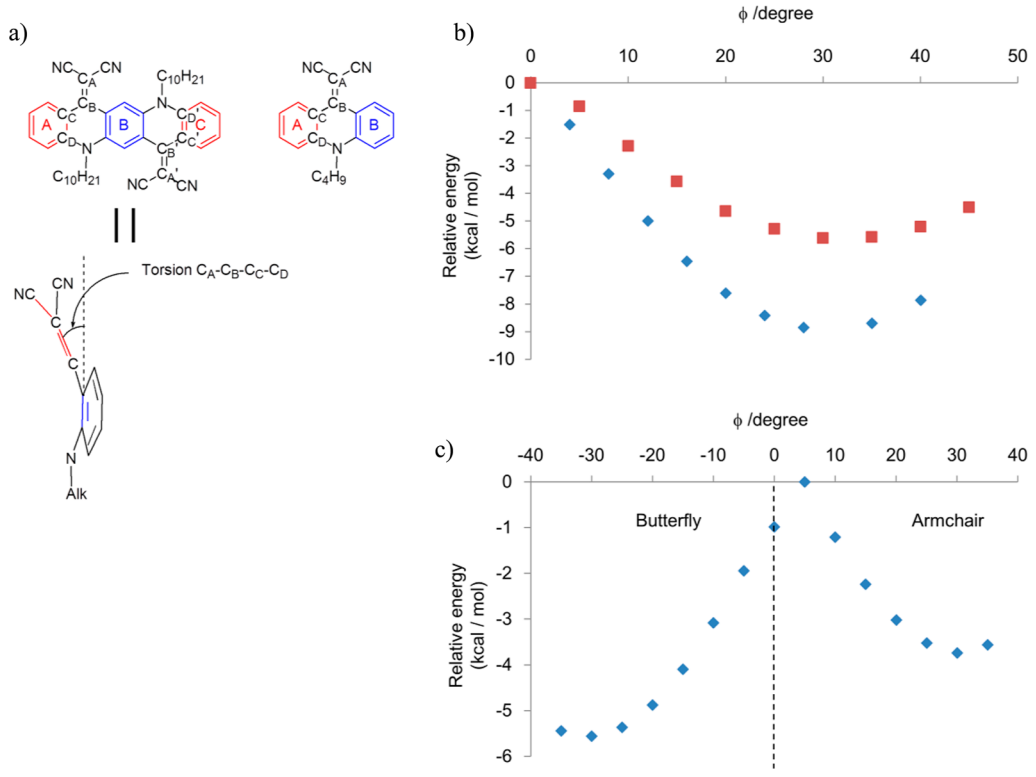

Figure 3. Potential energy curves for the molecular motions of **1** and **2**. Plots of relative energy against the torsion angles of $C_A-C_B-C_C-C_D$ (ϕ) based on DFT calculations using the B3LYP/6-31G* basis set. The alkyl groups were replaced by methyl groups in the calculations. (a) Definitions of torsion angles of $C_A-C_B-C_C-C_D$ (ϕ) and $C_A'-C_B'-C_C'-C_D'$ (ϕ') in molecules **1** and **2**. (b) Plots of the relative energies of molecules **1** (blue) and **2** (red) against the changes in the torsion angles $\phi = \phi'$. The symmetrical twisting of $C{=}C(CN)_2$ groups was calculated. (c) Plot of the relative energy of molecule **1** (blue) and ϕ with a fixed torsion angle of $\phi' = 31°$.

armchair conformation was only ~2 kcal mol^{-1}, and the potential energy barrier of this isomerization was very small (~6 kcal mol^{-1}). Thus, rapid transformation from the butterfly to the armchair conformation should occur around room temperature (Scheme 3). As the temperature increased, the ratio of armchair to curved, butterfly conformation increased based on the Gibbs free energy equation $\Delta G° = -RT \ln K$ and showed temperature-independent low-field shift at the H_a proton in the ^{1}H NMR spectrum. DFT calculations (B3LYP/6-31G*) estimated that the chemical shift of the H_a proton in the armchair conformation exists 0.27 ppm lower field than that of the curved, butterfly conformation, which was consistent with the experimental result.

Optical and Electrochemical Properties and Electrochromism. Figure 4 shows the UV−vis−NIR spectra of **1** and **2** in CH_2Cl_2. Because the molecular aggregation of **1** and **2** was not confirmed by concentration-dependent ^{1}H NMR (1−30 mM), the electronic spectra could be assigned to monomer species in solution. Numerous and complicated absorption bands were observed for **1** and **2**, which were associated with multiple D−A CT transitions. The low-energy absorption maxima of **1** and **2** were observed at 634 and 521 nm, respectively, which were red-shifted by 150 and 120 nm with respect to their corresponding precursors **3** and **4** (Figure S6 in the SI). The introduction of $C{=}C(CN)_2$ groups resulted in more effective intramolecular CT interaction between the electron-donating amino and electron-accepting $C{=}C(CN)_2$ groups compared to those in ketones **3** and **4**. The extended π system and multiple CT interactions in molecule **1** produced a greater red shift than was seen for molecule **2**.

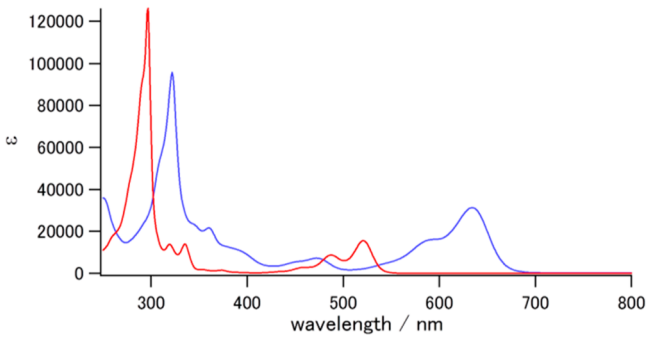

Figure 4. UV−vis−NIR spectra of **1** (blue) and **2** (red) in CH_2Cl_2.

The redox properties of **1** and **2** were evaluated by cyclic voltammogram (CV) measurements in CH_2Cl_2 and DMF (vs a reference electrode of Ag/AgCl). One-wave, two-electron reduction was observed for **1** at −0.80 V in CH_2Cl_2, and the corresponding oxidation wave was observed at −0.47 V (Figure S7 in the SI). The large difference between the reduction and oxidation potentials is consistent with dynamic conformational change within an electrochemical process. In contrast, the CV measurement of **2** showed one reversible redox process (Figure S8 in the SI). This indicates that the simultaneous two-electron reduction of **1** with a dynamic structural change prevents the generation of an anion radical species. The LUMO energy level of molecule **1** (−3.73 eV), based on the reduction potential,[24] was about 0.5 eV smaller than that of molecule **2** (−3.24 eV), which was associated with the size of the π-electron system and the intramolecular CT. The reduction peak of **1** in DMF

dx.doi.org/10.1021/jo501800g | J. Org. Chem. 2014, 79, 9669−9677

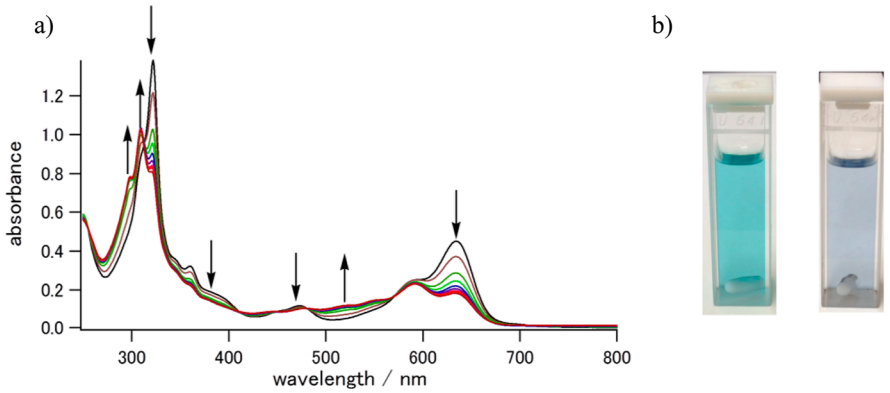

Figure 5. Changes in absorption spectra under the constant-current reduction of molecule **1** in CH_2Cl_2. (a) Constant-current electrolysis was carried out at 20 μA in a supporting electrolyte solution of Bu_4NBF_4 (0.1 M). The spectrum was measured every 24 min from a black (**1**) to a brown spectrum ($\mathbf{1}^{2-}$). (b) Change in the color of **1** from before (left) to after (right) electrolysis.

showed a 0.15 V anodic shift in contrast to that in CH_2Cl_2 (Figure S7 in the SI). Considering the subtle change in UV−vis spectra of **1** between DMF and CH_2Cl_2 (Figure S6 in the SI), this anodic shift can be accounted for by strong solvation of the dianionic species in DMF.

A large change in the conformation of neutral molecule **1** was expected upon two-electron reduction. The optimized molecular structure of dianion $\mathbf{1}^{2-}$ was almost planar (Figure 1c), whereas neutral species **1** shows a highly twisted structure. Thus, a drastic structural change upon electrochemical reduction should cause a change in the electronic nature of the molecule, which can be monitored by UV−vis spectroscopy. Figure 5 shows the changes in the electronic absorption spectra under constant-current electrolysis of **1** in CH_2Cl_2. The spectrum was measured every 24 min. During electrochemical reduction, a continuous spectral change with several isosbestic points at 313, 410, 448, 481, and 570 nm was observed, which reflected interconversion from the curved, butterfly-shaped π-bending structure of neutral **1** to the two-electron-reduced π-planar structure of $\mathbf{1}^{2-}$. Because an intermediate one-electron-reduced anion radical species was not confirmed in the CV measurement, the changes in the electronic spectra corresponded to the formation of a dianion state. The absorption maxima at ~295, ~310, and ~520 nm increased during the reduction process, whereas the intense low-energy absorption at ~635 nm decreased. These spectral changes were also confirmed by a change in the color of the solution from blue (neutral state) to blue-violet (dianion state), as shown in Figure 5b. Interestingly, a similar low-energy absorption bands at ~590 and ~635 nm have also been observed for structurally related indeno[1,2-*b*]fluorene, which has moderate singlet biradical character.[25] The contribution of the singlet biradical character of $\mathbf{1}^{2-}$ was estimated to be 37% by broken-symmetry UHF/6-31G(d) calculations[26] and the Yamaguchi scheme.[27] Therefore, dianion $\mathbf{1}^{2-}$ should have singlet biradical character. Its biradical character was additionally supported by a small energy separation between LUMO and NLUMO in dianion $\mathbf{1}^{2-}$ (8.0 kcal/mol; UB3LYP/6-31G*). A biradical species that can be accessed electrochemically by controlling the bias voltage would be an interesting optoelectronic material.

Two-Photon Absorption. Three π-conjugation pathways exist on the basis of the electron-donating and -accepting units in molecule **1**. (Scheme 4)[28] The alkylamine and $C{=}C(CN)_2$ units interact through the bent π conjugation (blue lines, Scheme 4) and/or linear conjugation (green lines, Scheme 4)

Scheme 4. Three π-Conjugation Pathways between Electron-Donating Amino and Electron-Accepting $C{=}C(CN)_2$ Units

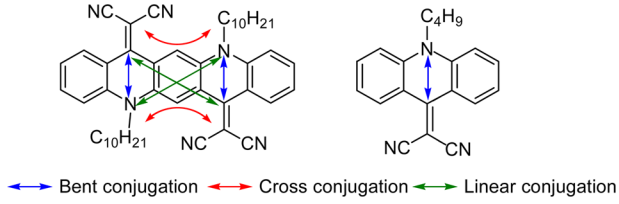

pathways, resulting in resonance and inductive effects. In contrast, cross conjugation (red lines, Scheme 4) was not connected to π-conjugation, resulting in only an inductive effect. Because the multiple D−A CT interactions and π-conjugation pathways within the molecule should play an important role in enhancing the TPA cross section, the TPA properties of **1** and **2** were investigated.

Figure 6 summarizes the TPA and one-photon absorption (OPA) spectra of **1** and **2** in DMSO.[29] TPA measurements

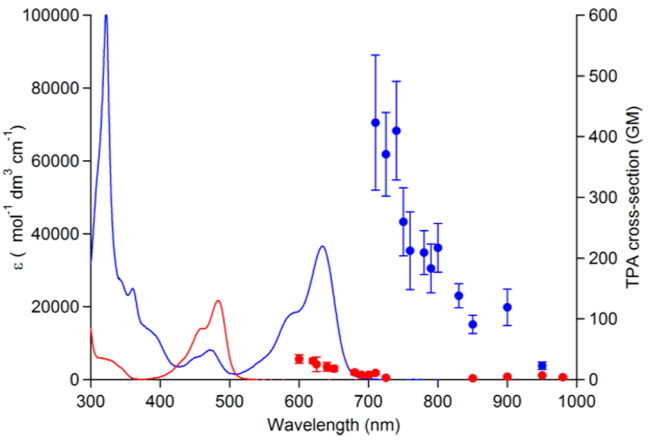

Figure 6. TPA (circle) and OPA (solid line) spectra of molecules **1** (blue) and **2** (red) in DMSO (~10^{-3} M).

were conducted in the area in which OPA is practically negligible. Both TPA spectra showed an increase in the TPA cross section with a decrease in the wavelength, which can be assigned to resonance-enhancement phenomena.[30] Although further enhancement of the TPA cross sections of **1** and **2** was expected at a shorter wavelength, OPA at shorter wavelengths

dx.doi.org/10.1021/jo501800g | J. Org. Chem. 2014, 79, 9669−9677

prevented their determination. The maximum TPA cross section of **1** was 423 GM (1 GM = 1×10^{-50} cm^4 s photon^{-1} molecule^{-1}) at 710 nm and **2** was 34 GM at 600 nm. Thus, the absolute magnitude of the TPA cross section of **1** was one order of magnitude larger than that of molecule **2**. Although resonance enhancement does not reflect the intrinsic electronic structure of a molecule, the TPA properties of **1** and **2** based on their electronic natures are considered in the discussion below. Although resonance enhancement significantly increases the TPA cross section in this study, it is not observed in all π-conjugated molecules. Resonance enhancement is typically observed in molecules with multiple absorption bands.[31] The intramolecular CT interactions in **1** and **2** resulted in multiple absorption bands, which effectively induced resonance enhancement with a relatively large TPA cross section. In a simple π molecule, the TPA cross section is proportional to the square of the number of π electrons based on theoretical predictions by Moreno and Kuzyk.[32] The numbers of π-electrons for **1** and **2** were 22 and 14, respectively, which enabled us to predict that the TPA cross section of **1** would be 2.5 times larger than that of **2** in terms of only the expansion of the π-electron system. However, the TPA cross section of **1** was actually 10-fold greater than that of molecule **2**, suggesting that a factor other than the number of π electrons enhances the TPA property of **1**. This factor enhancing the TPA cross section in **1** is likely due to the existence of multiple D−A CT pathways. The much longer D−A distance in the π-conjugated system increases the D−A transition dipole moment and the TPA cross section, which in turn helps to increase the TPA properties of **1** and **2**.

CONCLUSIONS

Single-crystal X-ray analysis revealed that dicyanomethylene-substituted quinacridone **1** had a curved, butterfly-shaped molecular structure in the solid state. Because the rotation of the C═C(CN)$_2$ groups in **1** and **2** was restricted by the C═C double-bond character, the steric hindrance between C═C(CN)$_2$ groups and neighboring hydrogen atoms on a benzene ring resulted in twisted molecular structures. The magnitude of the twist in **1** was larger than that in its acridone analog **2**, which demonstrated effective twisting around the C═C(CN)$_2$ groups. In contrast to the crystalline state, dynamic molecular motions of the curved, butterfly-shaped twisted structure in solution were confirmed by variable-temperature ^{1}H NMR and theoretical calculations, demonstrating that dynamic equilibrium existed between the curved, butterfly-shaped molecular conformation (global energy minimum) and a metastable armchair conformation, with an energy difference of ∼2 kcal mol^{-1}. The two-electron reduction of **1** in CH_2Cl_2 generated corresponding dianion **1**$^{2-}$, which had moderate biradical character. Theoretical calculations showed that dianion **1**$^{2-}$ had an almost planar molecular structure due to the conversion of C═C(CN)$_2$ double-bonding character to C−C(CN)$_2$ single bonds, allowing for possible rotation about the C−C bond. Such dynamic behavior between **1** and dianion **1**$^{2-}$ resulted in electrochromic behavior with reduction. The maximum TPA cross sections of **1** and **2** were 423 GM at 710 nm and 34 GM at 600 nm, respectively, in the resonance-enhancement region. Multiple D−A CT pathways in molecule **1** contributed to the increase in its TPA cross section. Such molecular designs have the potential to generate interesting TPA materials.

EXPERIMENTAL SECTION

General Methods. All chemical reactions were performed under a nitrogen atmosphere. Commercially available reagents and solvents were used without further purification. *N*-Butylacridone and *N*,*N*′-didecylquinacridone were prepared from acridone and quinacridone, respectively, according to the literature.[33] Chemical shifts (δ) were referenced to an internal standard of tetramethylsilane or residual nondeuterated solvent (^{1}H, 5.32 ppm for CD_2Cl_2; ^{13}C, 77.0 ppm for $CDCl_3$). Mass spectra were taken in FAB mode with a magnetic sector mass spectrometer. Infrared (IR, 400−4000 cm^{-1}) spectra were measured on a KBr pellet with a resolution of 4 cm^{-1}.

Preparation of Molecule ***1***. A mixture of *N*,*N*′-didecylquinacridone **3** (2.20 g, 3.71 mmol) and malononitrile (5.00 g, 75.7 mmol) in Ac_2O (100 mL) was stirred at 150 °C for 28 h. The resulting solution was cooled to room temperature, and the resulting precipitate was filtered. The obtained solid was recrystallized from MeCN to give **1** (1.39 g, 54%) as a dark-blue solid.

Mp: 189−190 °C. ^{1}H NMR (500 MHz, $CDCl_3$, 25 °C): δ 8.59 (s, 2H), 8.55 (d, J = 8.2 Hz, 2H), 7.75 (t, J = 7.7 Hz, 2H), 7.49 (d, J = 8.7 Hz, 2H), 7.34 (t, J = 7.7 Hz, 2H), 4.45 (t, J = 8.3 Hz, 4H), 2.03 (quint, J = 7.9 Hz, 4H), 1.64 (quint, J = 7.3 Hz, 4H), 1.50 (quint, J = 7.3 Hz, 4H), 1.44−1.25 (m, 20H), 0.90 (br t, J = 6.5 Hz, 6H). ^{13}C NMR (125 MHz, $CDCl_3$, 25 °C): δ 155.1, 139.3, 134.4, 133.6, 127.2, 122.8, 121.9, 117.6, 117.2, 116.8, 114.5, 111.6, 70.3, 49.2 31.9, 29.6, 29.5, 29.34, 29.29, 27.0, 26.8, 22.7, 14.1. IR: 2205, 1607, 1567, 1489, 1456, 1338, 1276, 1197, 754, 517 cm^{-1}. HRMS (FAB) calcd for $C_{46}H_{53}N_6$: 689.4332 [(M + H)$^+$]; found: 689.4331. Anal. Calcd for $C_{46}H_{52}N_6$: C, 80.19; H, 7.61; N, 12.20. Found: C, 79.82; H, 7.62; N, 12.08.

Preparation of Molecule ***2***. To a suspension of *N*-butylacridone **4** (1.00 g, 3.98 mmol) in Ac_2O (100 mL) was added malononitrile (2.62 g, 59.8 mmol). The mixture was stirred at 130 °C for 17 h. The resulting solution was cooled to room temperature, and the resulting precipitate was filtered and washed with Ac_2O to give **2** (684 mg, 57%), which was a yellow crystalline material.

Mp: 192−193 °C. ^{1}H NMR (500 MHz, $CDCl_3$, 25 °C): δ 8.55 (dd, J = 8.2, 1.3 Hz, 2H), 7.71 (ddd, J = 8.7, 7.0, 1.3 Hz, 2H), 7.49 (d, J = 8.7 Hz, 2H), 7.33 (ddd, J = 8.2, 7.0, 1.3 Hz, 2H), 4.34−4.29 (m, 2H), 2.00−1.92 (m, 2H), 1.62−1.53 (m, 2H), 1.09 (t, J = 7.5 Hz, 3H). ^{13}C NMR (125 MHz, $CDCl_3$, 25 °C): δ 156.3, 138.8, 133.5, 127.1, 121.9, 118.1, 117.6, 114.2, 68.1, 47.8, 28.8, 20.2, 13.8. IR: 2202, 2187, 1604, 1578, 1554, 1515, 1493, 1477, 1460, 1382, 1345, 1297, 1263, 1198, 1183, 1056, 758, 749, 661, 570 cm^{-1}. HRMS (FAB) calcd for $C_{20}H_{18}N_3$: 300.1501 [(M + H)$^+$]; found: 300.1498. Anal. Calcd for $C_{20}H_{17}N_3$: C, 80.24; H, 5.72; N, 14.04. Found: C, 80.32; H, 5.83; N, 14.01.

X-ray Structural Analysis. Temperature-dependent crystallographic data (Table 2) were collected using a diffractometer equipped with a rotating anode fitted with a multilayer confocal optic using Cu Kα (λ = 1.54187 Å) radiation. Structural refinements were carried out using the full-matrix least-squares method on F^2. Calculations were performed using the Crystal Structure and SHELEX software packages.[34] Except for the hydrogen atom, parameters were refined using anisotropic temperature factors.

Computational Methods. DFT calculations were performed with the Gaussian 09 program package.[35] The geometries of the molecules were optimized using the B3LYP/6-31G* basis set. Stationary points were assessed by a vibrational frequency analysis. The relative energies of **1** and **2** were calculated using an optimized structure with a fixed corresponding torsion angle ϕ (and ϕ'). Singlet biradical character was estimated using the broken-symmetry UHF/6-31G* method.

Two-Photon Absorption Spectra. TPA spectra were measured using open-aperture Z-scan measurements.[36] A femtosecond pulsed beam from an optical parametric amplifier pumped by a beam from a regenerative amplifier was used as the light source. The typical pulse duration was 150−200 fs, and the repetition rate was 1 kHz. The incident beam was focused by a plano-convex lens (f = 150 nm). The sample solution was scanned along the incident beam axis. The average peak power was varied from 0.01 to 0.4 mW, corresponding to one-axis peak powers of 6 to 240 GW/cm^2. The two-photon

dx.doi.org/10.1021/jo501800g | J. Org. Chem. 2014, 79, 9669−9677

Table 2. Crystal Data, Data Collection, and Reduction Parameters for Crystals 1 and 2

	1	2
chemical formula	$C_{46}H_{52}N_6$	$C_{20}H_{17}N_3$
formula weight	688.96	299.37
space group	$P\bar{1}$ (No. 2)	$P2_1$ (No. 4)
a, Å	8.9013(2)	10.1013(2)
b, Å	13.2462(3)	7.05282(15)
c, Å	13.2462(3)	10.41517(19)
α, deg	84.1372(7)	
β, deg	81.9146(7)	92.2668(13)
γ, deg	68.2867(7)	
V, Å^3	1920.21(6)	741.42(3)
Z	2	2
D_{calc}, g cm^{-1}	1.191	1.341
μ, cm^{-1}	5.426	6.283
refs meas	22 122	8522
indep refls	6897	2610
refls used	6897	2610
R^a	0.0831	0.0454
R_w $(F^2)^a$	0.2827	0.1179
GOF	1.113	1.024

$^aR = \Sigma||F_o| - |F_c||/\Sigma|F_o|$ and $R_w = (\Sigma\omega(|F_o| - |F_c|)^2/\Sigma\omega F_o^2)^{1/2}$.

absorbance (q_0) was obtained by a curve fit to the trace of the open-aperture Z-scan signal with a previously described theoretical equation,[30] assuming a spatial and temporal Gaussian beam. The parameter q_0 was defined as $q_0 = \beta I_0 L_{eff}$, where β, I_0, and L_{eff} denote the TPA coefficient, incident power, and effective path length, respectively. The TPA cross section ($\sigma^{(2)}$) was calculated from $\sigma^{(2)} = \hbar\omega\beta/N$, where $\hbar\omega$ is the photon energy of the incident light and N denotes the molecule number density. If the transmittance changes observed by the Z-scan measurements were purely TPA-dependent and not reliant on any other nonlinear optical process, then the plot of q_0 versus I_0 becomes linear. We evaluated $\sigma^{(2)}$ from β, which was determined in a power range when the proportional relationship between q_0 and I_0 had been confirmed. Z-scan measurements of **1** and **2** were performed using a DMSO solution at a concentration of 10^{-3} mol L^{-1}. At this concentration, dyes did not form aggregates.

■ ASSOCIATED CONTENT

Supporting Information

Crystal data (CIF) of **1** and **2**. Detailed crystal structure and ORTEP drawings of **1** and **2**. Concentration-dependent ^{1}H NMR spectra of **1** in $CDCl_3$. UV−vis spectra of **1** in DMF and **3** and **4** in CH_2Cl_2. Cyclic voltammograms of **1** and **2** in CH_2Cl_2 and DMF. ^{1}H and ^{13}C NMR spectra of **1** and **2**. Cartesian coordinates for the optimized structures of **1** (curved, butterfly structure and armchair structure) and $\mathbf{1}^{2-}$. This material is available free of charge via the Internet at http://pubs.acs.org.

■ AUTHOR INFORMATION

Corresponding Authors

*E-mail: takeda@tagen.tohoku.ac.jp.
*E-mail: akuta@tagen.tohoku.ac.jp.

Notes

The authors declare no competing financial interest.

■ ACKNOWLEDGMENTS

This work was supported by JSPS KAKENHI (no. 26410034).

■ REFERENCES

(1) (a) Garcia-Garibay, M. A. *Proc. Natl. Acad. Sci. U.S.A.* **2005**, *102*, 10771−10776. (b) Khuong, T.-A. V.; Nuñez, J. E.; Godinez, C. E.; Garcia-Garibay, M. A. *Acc. Chem. Res.* **2006**, *39*, 413−422.

(2) (a) Horike, S.; Matsuda, R.; Tanaka, D.; Matsubara, S.; Mizuno, M.; Endo, K.; Kitagawa, S. *Angew. Chem., Int. Ed.* **2006**, *45*, 7226−7230. (b) Zhou, W.; Yildirim, T. *Phys. Rev. B* **2006**, *B74*, 180301. (c) Winston, E. B.; Lowell, P. J.; Vacek, J.; Chocholoušová, M. J.; Michl, J.; Price, J. C. *Phys. Chem. Chem. Phys.* **2008**, *10*, 5188−5191. (d) Mugridge, J. S.; Szigethy, G.; Bergman, R. G.; Raymond, K. N. *J. Am. Chem. Soc.* **2010**, *132*, 16256−16264.

(3) (a) Sato, D.; Akutagawa, T.; Takeda, S.; Noro, S.; Nakamura, T. *Inorg. Chem.* **2007**, *46*, 363−365. (b) Akutagawa, T.; Sato, D.; Koshinaka, H.; Aonuma, M.; Noro, S.; Takeda, S.; Nakamura, T. *Inorg. Chem.* **2008**, *47*, 5951−5962. (c) Akutagawa, T.; Sato, D.; Ye, Q.; Endo, T.; Noro, S.; Takeda, S.; Nakamura, T. *Dalton Trans.* **2010**, *39*, 8219−8227. (d) Ye, Q.; Takahashi, K.; Hoshino, N.; Kikuchi, T.; Akutagawa, T.; Noro, S.; Takeda, S.; Nakamura, T. *Chem.—Eur. J.* **2011**, *17*, 14442−14449.

(4) Akutagawa, T.; Koshinaka, H.; Sato, D.; Takeda, S.; Noro, S.; Takahashi, H.; Kumai, R.; Tokura, Y.; Nakamura, T. *Nat. Mater.* **2009**, *8*, 342−347.

(5) (a) Brouwer, A. M.; Frochot, C.; Gatti, F. G.; Leigh, D. A.; Mottier, L.; Paolucci, F.; Roffia, S.; Wurpel, G. W. H. *Science* **2001**, *291*, 2124−2128. (b) Crowley, J. D.; Goldup, S. M.; Lee, A.-L.; Leigh, D. A.; McBurney, R. T. *Chem. Soc. Rev.* **2009**, *38*, 1530−1541.

(6) (a) Iwamura, H.; Mislow, K. *Acc. Chem. Res.* **1988**, *21*, 175−182. (b) Frantz, D. K.; Linden, A.; Baldridge, K. K.; Siegel, J. S. *J. Am. Chem. Soc.* **2012**, *134*, 1528−1535.

(7) (a) Sakurai, H.; Daiko, T.; Hirao, T. *Science* **2003**, *301*, 1878. (b) Amaya, T.; Sakane, H.; Munenishi, T.; Hirao, T. *Chem. Commun.* **2008**, 765−767. (c) Amaya, T.; Nakata, T.; Hirao, T. *J. Am. Chem. Soc.* **2009**, *131*, 10810−10811. (d) Seiders, T. J.; Baldridge, K. K.; Grube, G. H.; Siegel, J. S. *J. Am. Chem. Soc.* **2001**, *123*, 517−525. (e) Higashibayashi, S.; Tsuruoka, R.; Soujanya, Y.; Purushotham, U.; Sastry, G. N.; Seki, S.; Ishikawa, T.; Toyota, S.; Sakurai, H. *Bull. Chem. Soc. Jpn.* **2012**, *85*, 450−467.

(8) (a) Monk, P. M. S.; Mortimer, R. J.; Rosseinsky, D. R. *Electrochromism: Fundamentals and Applications*; John Wiley and Sons: New York, 2008. (b) Monk, P.; Mortimer, R.; Rosseinsky, D. *Electrochromism and Electrochromic Devices*; Cambridge University Press: New York, 2007. (c) Suzuki, T.; Ohta, E.; Kawai, H.; Fujiwara, K.; Fukushima, T. *Synlett* **2007**, 851−869.

(9) (a) Hünig, S.; Kemmer, M.; Wenner, H.; Perepichka, I. F.; Bäuerle, P.; Emge, A.; Gescheid, G. *Chem.—Eur. J.* **1999**, *5*, 1969−1973. (b) Hünig, S.; Kemmer, M.; Wenner, H.; Barbosa, F.; Gescheidt, G.; Perepichka, I. F.; Bäuerle, P.; Emge, A.; Peters, K. *Chem.—Eur. J.* **2000**, *6*, 2618−2632. (c) Hünig, S.; Perepichka, I. F.; Kemmer, M.; Wenner, H.; Bäuerle, P.; Emge, A. *Tetrahedron* **2000**, *56*, 4203−4211.

(10) (a) Suzuki, T.; Nishida, J.; Tsuji, T. *Angew. Chem., Int. Ed. Engl.* **1997**, *36*, 1329−1331. (b) Suzuki, T.; Nishida, J.; Tsuji, T. *Chem. Commun.* **1998**, 2193−2194. (c) Suzuki, T.; Migita, A.; Higuchi, H.; Kawai, H.; Fujiwara, K.; Tsuji, T. *Tetrahedron Lett.* **2003**, *44*, 6837−6840. (d) Suzuki, T.; Ishigaki, Y.; Iwai, T.; Kawai, H.; Fujiwara, K.; Ikeda, H.; Kano, Y.; Mizuno, K. *Chem.—Eur. J.* **2009**, *15*, 9434−9441. (e) Suzuki, T.; Wada, K.; Ishigaki, Y.; Yoshimoto, Y.; Ohta, E.; Kawai, H.; Fujiwara, K. *Chem. Commun.* **2010**, *46*, 4100−4102. (f) Highchi, H.; Ohta, E.; Kawai, H.; Fujiwara, K.; Tsuji, T.; Suzuki, T. *J. Org. Chem.* **2003**, *68*, 6605−6610. (g) Ohta, E.; Higuchi, H.; Kawai, H.; Fujiwara, K.; Suzuki, T. *Org. Biomol. Chem.* **2005**, *3*, 3024−3031. (h) Iwashita, S.; Ohta, E.; Higuchi, H.; Kawai, H.; Fujiwara, K.; Ono, K.; Takenaka, M.; Suzuki, T. *Chem. Commun.* **2004**, 2076−2077. (i) Suzuki, T.; Sakano, Y.; Iwai, T.; Iwashita, S.; Miura, Y.; Katoono, R.; Kawai, H.; Fujiwara, K.; Tsuji, Y.; Fukushima, T. *Chem.—Eur. J.* **2013**, *19*, 117−123.

(11) Higuchi, H.; Ichioka, K.; Kawai, H.; Fujiwara, K.; Ohkita, M.; Tsuji, T.; Suzuki, T. *Tetrahedron Lett.* **2004**, *45*, 3027−3030.

(12) (a) Wang, J.; Zhao, Y.; Dou, C.; Sun, H.; Xu, P.; Ye, K.; Zhang, J.; Jiang, S.; Li, F.; Wang, Y. *J. Phys. Chem. B* **2007**, *111*, 5082−5089.

See also (b) Yu, D.; Peng, T.; Zhang, H.; Bi, H.; Zhang, J.; Wang, Y. *New J. Chem.* **2010**, *34*, 2213−2219.
(13) (a) Chen, J. J.-A.; Chen, T. L.; Kim, B.; Poulsen, D. A.; Mynar, J. L.; Fréchet, J. M. J.; Ma, B. *ACS Appl. Mater. Interfaces* **2010**, *2*, 2679−2686. (b) Pho, T. V.; Zalar, P.; Garcia, A.; Nguyen, T.-Q.; Wudl, F. *Chem. Commun.* **2010**, *46*, 8210−8212.
(14) Fattori, V.; Di Marco, P.; Giro, G.; Kalinowski, J. *Mol. Cryst. Liq. Cryst.* **1992**, *211*, 313−319.
(15) Review: Pawlicki, M.; Collins, H. A.; Denning, R. G.; Anderson, H. L. *Angew. Chem., Int. Ed.* **2009**, *48*, 3244−3266.
(16) (a) Kamada, K.; Ohta, K.; Kubo, T.; Shimizu, A.; Morita, Y.; Nakasuji, K.; Kishi, R.; Ohta, S.; Furukawa, S.; Takahashi, H.; et al. *Angew. Chem., Int. Ed.* **2007**, *46*, 3544−3546. (b) Kamada, K.; Fuku-en, S.; Minamide, S.; Ohta, K.; Kishi, R.; Nakano, M.; Matsuzaki, H.; Okamoto, H.; Higashikawa, H.; Inoue, K.; et al. *J. Am. Chem. Soc.* **2013**, *135*, 232−241.
(17) (a) Drobizhev, M.; Stepanenko, Y.; Rebane, A.; Wilson, C. J.; Screen, T. E. O.; Anderson, H. L. *J. Am. Chem. Soc.* **2006**, *128*, 12432−12433. (b) Drobizhev, M.; Stepanenko, Y.; Dzenis, Y.; Karotki, A.; Rebane, A.; Taylor, P. N.; Anderson, H. L. *J. Phys. Chem. B* **2005**, *109*, 7223−7236. (c) Yoon, M.-C.; Noh, S. B.; Tsuda, A.; Nakamura, Y.; Osuka, A.; Kim, D. *J. Am. Chem. Soc.* **2007**, *129*, 10080−10081.
(18) For example, (a) Albota, M.; Beljonne, D.; Brédas, J.-L.; Ehrlich, J. E.; Fu, J.-Y.; Heikal, A. A.; Hess, S. E.; Kogej, T.; Levin, M. D.; Marder, S. R.; et al. *Science* **1998**, *281*, 1653−1656. (b) Iwase, Y.; Kamada, K.; Ohta, K.; Kondo, K. *J. Mater. Chem.* **2003**, *13*, 1575−1581. (c) Shao, P.; Huang, B.; Chen, L.; Liu, Z.; Qin, J.; Gong, H.; Ding, S.; Wang, Q. *J. Mater. Chem.* **2005**, *15*, 4502−4506. (d) Kim, O.-K.; Lee, K. S.; Woo, H. Y.; Kim, K. S.; He, G. S.; Swiatkiewicz, J.; Prasad, P. N. *Chem. Mater.* **2000**, *12*, 284−286.
(19) Zhou, T.; Jia, T.; Kang, B.; Li, F.; Fahlman, M.; Wang, Y. *Adv. Energy Mater.* **2011**, *1*, 431−439.
(20) (a) Ye, K.; Wang, J.; Sun, H.; Liu, Y.; Mu, Z.; Li, F.; Jiang, S.; Zhang, J.; Zhang, H.; Wang, Y.; et al. *J. Phys. Chem. B* **2005**, *109*, 8008−8016. (b) Fan, Y.; Zhao, Y.; Ye, L.; Li, B.; Yang, G.; Wang, Y. *Cryst. Growth Des.* **2009**, *9*, 1421−1430. (c) Fan, Y.; Song, W.; Yu, D.; Ye, K.; Zhang, J.; Wang, Y. *CrystEngComm* **2009**, *11*, 1716−1722. (d) Zhao, Y.; Mu, X.; Bao, C.; Fan, Y.; Zhang, J.; Wang, Y. *Langmuir* **2009**, *25*, 3264−3270. (e) Mizuguchi, J.; Senju, T. *Acta Crystallogr.* **2003**, *E59*, o232−o233.
(21) Schubert, U.; Hünig, S.; Aumüller, A. *Liebigs Ann. Chem.* **1985**, 1216−1222.
(22) Sun, H.; Ye, K.; Wang, C.; Qi, H.; Li, F.; Wang, Y. *J. Phys. Chem. A* **2006**, *110*, 10750−10756.
(23) (a) Jensen, F. R.; Noyce, D. S.; Sederholm, C. H.; Berlin, A. J. *J. Am. Chem. Soc.* **1962**, *84*, 386−389. (b) Anet, F. A. L.; Bourn, A. J. R. *J. Am. Chem. Soc.* **1967**, *89*, 760−768.
(24) Liu, Y.; Liu, M. S.; Jen, A. K.-Y. *Acta Polym.* **1999**, *50*, 105−108.
(25) (a) Chase, D. T.; Rose, B. D.; McClintock, S. P.; Zakharov, L. N.; Haley, M. M. *Angew. Chem., Int. Ed.* **2011**, *50*, 1127−1130. (b) Chase, D. T.; Fix, A. G.; Rose, B. D.; Weber, C. D.; Nobusue, S.; Stockwell, C. E.; Zaharov, L. N.; Lonergan, M. C.; Haley, M. M. *Angew. Chem., Int. Ed.* **2011**, *50*, 11103−11106. (c) Chase, D. T.; Fix, A. G.; Kang, S. J.; Rose, B. D.; Weber, C. D.; Zhong, Y.; Zakharov, L. N.; Lonergan, M. C.; Nuckolls, C.; Haley, M. M. *J. Am. Chem. Soc.* **2012**, *134*, 10349−10352.
(26) (a) Döhnert, D.; Koutecký, J. *J. Am. Chem. Soc.* **1980**, *102*, 1789−1796. (b) Jung, Y.; Head-Gordon, M. *ChemPhysChem* **2003**, *4*, 522−525.
(27) Yamaguchi, K. *Chem. Phys. Lett.* **1975**, *33*, 330−335.
(28) For a definition of conjugation pathways, see Marsden, J. A.; Miller, J. J.; Shirtcliff, L. D.; Haley, M. M. *J. Am. Chem. Soc.* **2005**, *127*, 2464−2476.
(29) The UV−vis spectra of **1** and **2** showed the same absorption properties in DMSO as in CH_2Cl_2.
(30) Kamada, K.; Ohta, K.; Iwase, Y.; Kondo, K. *Chem. Phys. Lett.* **2003**, *372*, 386−393.
(31) (a) Hirakawa, S.; Kawamata, J.; Suzuki, Y.; Tani, S.; Murafuji, T.; Kasatani, K.; Antonov, L.; Kamada, K.; Ohta, K. *J. Phys. Chem. A* **2008**, *112*, 5198−5207. (b) Drobizhev, M.; Stepanenko, Y.; Dzenis, Y.; Karotki, A.; Rebane, A.; Taylor, P. N.; Anderson, H. L. *J. Am. Chem. Soc.* **2004**, *126*, 15352−15353. (c) Moritomo, H.; Nakagawa, K.; Sugihara, H.; Suzuki, Y.; Kawamata, J. *Chem. Lett.* **2013**, *43*, 441−443.
(32) Moreno, J. P.; Kuzyk, M. G. *J. Chem. Phys.* **2005**, *123*, 194101.
(33) (a) Acheson, R. M.; Constable, E. C. *J. Chem. Soc., Chem. Commun.* **1980**, 1065−1066. (b) Liu, J.; Gao, B.; Cheng, Y.; Xie, Z.; Geng, Y.; Wang, L.; Jing, X.; Wang, F. *Macromolecules* **2008**, *41*, 1162−1167.
(34) Sheldrick, G. M. *Acta Crystallogr.* **2008**, *64A*, 112−122.
(35) Frisch, M. J.; Trucks, G. W.; Schlegel, H. B.; Scuseria, G. E.; Robb, M. A.; Cheeseman, J. R.; Scalmani, G.; Barone, V.; Mennucci, B.; Petersson, G. A.; et al. *Gaussian 09*, Revision C 01; Gaussian, Inc.: Wallingford, CT, 2009.
(36) Sheik-Bahae, M.; Said, A. A.; Wei, T.-H.; Hagan, D. J.; Stryland, E. W. V. *IEEE J. Quantum Electron.* **1990**, *26*, 760−769.